RESEARCH ARTICLE

**ADVANCED
PHOTONICS
RESEARCH**
Open Access

www.adpr-journal.com

Room Temperature Polariton Lasing in Ladder-Type Oligo(*p*-Phenylene)s with Different π-Conjugation Lengths

Mengjie Wei, Mei Fang, Sai Kiran Rajendran, Wen-Yong Lai,* Graham A. Turnbull,* and Ifor D. W. Samuel*

Polariton lasing is coherent emission that originates from macroscopic accumulation of polariton population in the ground state and is a promising route toward efficient coherent light sources as population inversion is not necessary. Unlike most Wannier–Mott excitons in inorganic semiconductors, Frenkel excitons created in organic semiconductors have high oscillator strength and high exciton binding energy, which sustain stable exciton–polaritons at room temperature. Herein, room temperature polariton lasing from a novel class of ladder-type oligo(*p*-phenylene)s is demonstrated. The polariton lasers exhibit a nonlinear increase of their spectrally integrated emission, a reduction in spectral linewidth, blueshift of emission peaks, and long-range spatial coherence when the pump fluence is increased above threshold. By tuning the π-conjugation length of the molecular structure, the polariton lasing wavelength can be changed from 430 to 457 nm. Optically pumped thresholds of 12 and 17 $\mu J\,cm^{-2}$ are observed, which are among the lowest values reported for polariton lasing in organic semiconductors.

1. Introduction

Exciton–polaritons are quasi-particles that arise from strong coupling between excitons and cavity photons.[1] Under appropriate conditions, these bosonic particles can undergo stimulated scattering to the ground state of the lower polariton branch (LPB), generating coherent light without the need for population inversion. These devices are called polariton lasers[2,3] and have been reported experimentally to have the energy thresholds two to three orders of magnitude lower than that of photon lasers in the same cavity configuration.[4,5] Nonlinear behavior related to interactions between polaritons in such systems is also attractive for studying non-equilibrium Bose–Einstein condensation[6] and superfluidity.[7] A broad spectrum of active layers is currently being investigated among inorganic semiconductors (such as GaN,[8] ZnO,[9] and perovskites[10,11]), organic semiconductors, and hybrid materials.[12–15] Organic semiconductors contain localized Frenkel excitons with high exciton binding energy (of several hundreds of meV) and high oscillator strength. These attractive properties enable demonstration of strong coupling at room temperature.[16] In addition, their simple fabrication and broadband tunability can help realize large area and multi-purpose polariton devices. There has been significant activity dedicated to organic polaritonics in the last decade, and several organic materials have now been reported to show room temperature polariton lasing, including the anthracene single crystal,[17] conjugated polymers,[6,18] oligofluorenes,[19,20] fluorescent proteins,[21,22] and fluorescent dyes.[23,24]

In this work, we report the demonstration of polariton lasing in two novel ladder-type oligo(*p*-phenylene)s, having donor–π–acceptor architectures end-capped with diphenylamine and fluorine units (2L-F and 4L-F). **Figure 1**a shows their molecular structures. The fused phenylene rings give extensive π-conjugation along the rigid backbone, whereas solubilizing side groups enable simple processing from solution. These structural properties result in narrow and well-defined exciton transitions, outstanding thermal and photochemical stabilities, and high photoluminescence quantum yield (PLQY).[25] These two materials also exhibit very high exciton binding energy[26] and absorption oscillator strength,[27] which should be beneficial to the formation of stable room-temperature exciton–polaritons.

We fabricated planar distributed Bragg reflector (DBR) cavities containing 2L-F and 4L-F to explore their potential for polariton lasing. The strongly coupled cavities show polariton lasing in both materials, with the wavelength tuned (by ≈27 nm) by

M. Wei, Dr. S. K. Rajendran, Prof. G. A. Turnbull, Prof. I. D. W. Samuel
Organic Semiconductor Center
SUPA, School of Physics and Astronomy
University of St Andrews
St Andrews KY16 9SS, UK
E-mail: gat@st-andrews.ac.uk; idws@st-andrews.ac.uk

M. Fang, Prof. W.-Y. Lai
Key Laboratory for Organic Electronics and Information Displays, Institute of Advanced Materials (IAM)
Nanjing University of Posts & Telecommunications
9 Wenyuan Road, Nanjing 210023, China
E-mail: iamwylai@njupt.edu.cn

Prof. W.-Y. Lai
Shaanxi Institute of Flexible Electronics (SIFE)
Northwestern Polytechnical University (NPU)
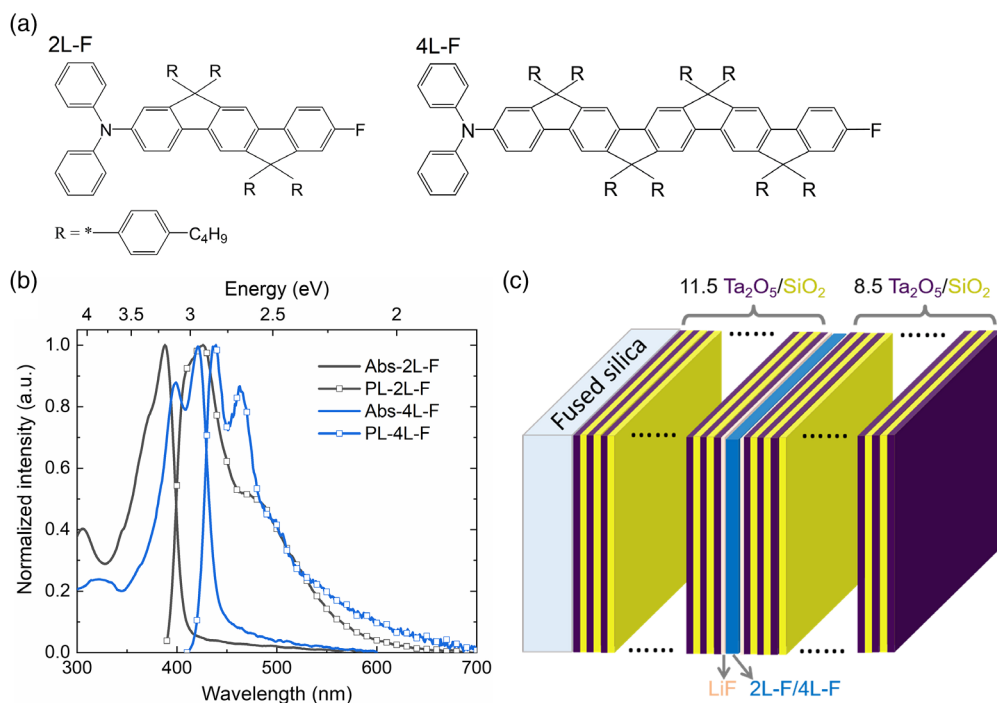127 West Youyi Road, Xi'an 710072, Shaanxi, China

Figure 1. a) Molecular structures of 2L-F and 4L-F. b) Absorption (solid line) and PL (line symbol) spectra of 2L-F (black) and 4L-F (blue) bare films on fused silica substrates. c) Schematic of the planar DBR microcavities.

changing the π-conjugation length of the molecular backbone from 2L-F to 4L-F. We find that the thresholds of these cavities are relatively low and comparable with the lowest threshold that has been reported for organic semiconductors.[20]

2. Results and Discussion

Figure 1b shows the absorption and photoluminescence (PL) spectra of neat films of 2L-F and 4L-F. The absorption spectrum of 2L-F exhibits a pronounced peak at 388 nm and a shoulder at 374 nm, with a full width at half maximum (FWHM) of 44 nm. The PL spectrum of 2L-F shows the two vibrational peaks at 427 and 472 nm with an overall FWHM of 78 nm. In comparison, the absorption peaks of 4L-F are more distinct, which may be attributed to the more rigid molecular structure of 4L-F compared with 2L-F. The lowest energy excitonic transition is at 421 nm with an FWHM of 18 nm, and its vibronic replica is at 399 nm with a linewidth of 26 nm, whereas the emission is symmetrical with the absorption spectrum, with peaks are at 438 and 463 nm. Both absorption and emission spectra redshift with an increasing number of bridged phenylene rings. The PLQY of solid-state films of 2L-F and 4L-F was measured to have the values of 24% and 28%, respectively.

As shown in Figure 1c, the microcavities consist of a single layer of spin-coated 2L-F or 4L-F as the active layer, and 20 nm thick lithium fluoride (LiF) layers were thermally deposited both prior to and after the spin-coating process to protect active layers from plasma damage[28] and penetration of ions.[29] In our previous study, it was found that the protective LiF layer prevented degradation of PLQY in organic films due to

subsequent sputter deposition.[20] The bottom and top DBRs were designed to be highly reflective across both absorption and emission spectra of 2L-F or 4L-F, while still having relatively high transmittance to the pump laser wavelength. The quality factors were estimated from reflectivity of the bottom and top DBRs to be 302 for the 2L-F cavity and 356 for the 4L-F cavity, corresponding, respectively, to the cavity photon lifetimes of 78 and 94 fs as given by

$$\tau_{\mathrm{photon}} = 2d/[c(1 - R_1 R_2)] \tag{1}$$

where d is the optical length between the two DBR mirrors, and R_1 and R_2 are the reflectivity of the mirrors.

White light p-polarized angle-resolved reflectivity maps for a 114 nm thick 2L-F cavity are shown in **Figure 2**a (with additional reflectivity data in Figure S1 and S2, Supporting Information), presenting the measured reflectivity spectra from 20° to 74°. It is evident that there are two modes at resonance between the exciton transition energy at 3.2 eV and the cavity photon mode. These two dispersive features are attributed as the upper polariton branch (UPB) and the LPB, which are signatures of strong coupling between the exciton transition and the cavity photon mode. The measured reflectivity minima are matched with a standard two-level coupled oscillator model. The solid lines trace the matched dispersion of the UPB and LPB, and the dashed lines represent the dispersionless uncoupled excitons and the parabolic cavity photon mode obtained from the oscillator model. The Rabi splitting was extracted to be 220 meV with a cavity detuning of −269 meV and an exciton fraction of 11% at the LPB minimum (Figure S3a, Supporting Information) for the 2L-F cavity.
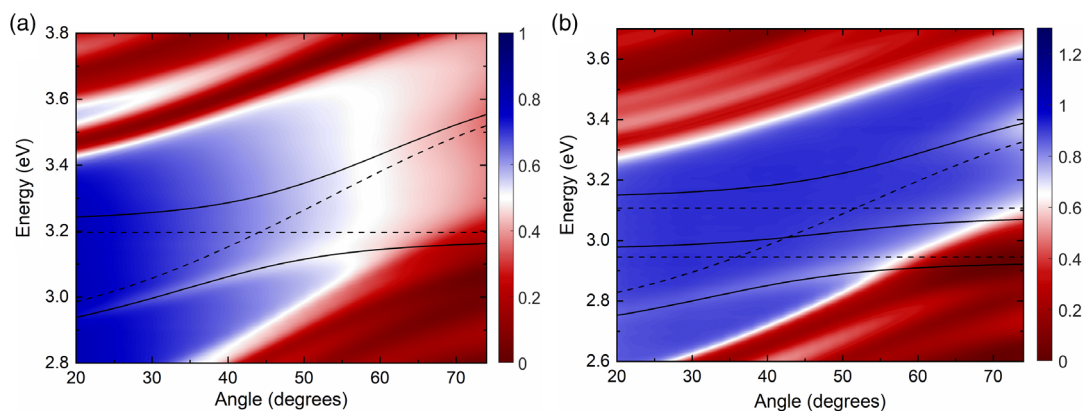
**ADVANCED
SCIENCE NEWS**

www.advancedsciencenews.com

**ADVANCED
PHOTONICS
RESEARCH**
Open Access

www.adpr-journal.com

Figure 2. *P*-polarized angle-resolved reflectivity maps for a) 2L-F and b) 4L-F microcavities. Solid lines are matched results to coupled oscillator models, whereas dashed lines are uncoupled exciton and cavity photon modes.

Figure 2b shows the angle-resolved reflectivity contour map for a 118 nm thick 4L-F cavity. We find that the measured reflectivity minima cannot be simply described by a two-level coupled oscillator model, even though an anticrossing is observed. As shown in Figure 1b, there are two discrete excitonic transitions in the 4L-F solid state film, which each may contribute to strong coupling with the cavity photon mode. Therefore, reflectivity spectra of the 4L-F cavity might be expected to manifest two anticrossings, one between the (0, 0) excitonic transition at 2.95 eV and the cavity photon mode and the other between the (0, 1) excitonic transition at 3.11 eV and the cavity photon mode. In this case where two exciton modes couple to the photon mode, we try instead to fit the dispersion with a three-level coupled oscillator model. The splittings are found to be 220 meV between the UPB and the middle polariton branch (MPB), and 180 meV between the MPB and the LPB. The photon mode is 172 meV red detuned from the lowest energy excitonic transition. The overall splitting between the UPB and LPB is increased compared with that of the 2L-F cavity results due to the additional exciton state coupled to the photon mode. At $k_{//} = 0$, the wavefunction of the LBP has 82% photonic, 12% (0, 0) excitonic, and 6% (0, 1) excitonic wavefunction contributions, as shown in Figure S3b, Supporting Information. It should be noted that we did not observe the dispersion of an MPB in the 4L-F cavity due to absorption from subradiant exciton states in the disordered system.[19,30,31] This is consistent with the calculated photon fraction of each polariton branch, as shown in Figure S3b, Supporting Information. The MPB has photon fraction less than 25% at all angles, which makes it couple poorly to radiation, making it difficult to observe.

The microcavities were subsequently pumped by a pulsed laser at 343 nm with a pulse duration of 200 fs and the repetition rate of 5 kHz. A Fourier imaging microscope in a transmission configuration was used to record the angle-resolved PL from microcavities at different pump fluences. The results are shown in **Figure 3**a,c for 2L-F and 4L-F cavities. Only negative (for low pump fluence) or positive (for high pump fluence) angles are plotted here because of the symmetry in the angle-resolved PL maps around normal incidence. At low pump fluence, emission

follows the LPB dispersion obtained from angle-resolved reflectivity spectra in Figure 2. This indicates that the two cavities are in the strong coupling regime at low pump fluence. The bare photon modes of these cavities obtained from coupled oscillator models are plotted as white dashed lines and are detuned away from the emission band. The LPB emission in each cavity is most intense at the bottom of the branch and gradually decreases in intensity at higher angles, which is consistent with the reduction of photon fraction along the LPB toward high angles as calculated in Figure S3, Supporting Information. On increasing pump fluence, we observe a collapse of the LPB emission to the bottom of the branch for both 2L-F and 4L-F cavities, as shown in the right halves of Figure 3a,c. The macroscopic accumulation of polariton population at the bottom of the LPB is a key feature of polariton lasing.

The integrated intensity (between 2.92 and 2.87 eV) of emission spectra at $k_{//} = 0$ from the 2L-F cavity, the FWHM, and the peak energy shift referenced to the PL spectrum at the lowest excitation density is plotted as a function of incident pump fluence in Figure 3b. We find that the spectrally integrated intensities increase first sub-linearly below threshold, and then super-linearly above a threshold of 63 µJ cm^{-2}. The linewidth reduces from 8.9 to 0.8 meV and subsequently broadens with the further increase of the pump fluence. Spectral broadening has previously been seen in other studies of both organic[19] and inorganic[32] cavities, where the reason has been attributed to a polariton self-interaction-induced decoherence process and multi-mode lasing.[33,34] The individual emission spectra of 2L-F cavity at $k_{//} = 0$ extracted from angle-resolved PL maps recorded at various pump fluences are shown in Figure S4a–c, Supporting Information. These show that the initial gradual broadening above threshold results from a broadening of an individual peak, before multi-mode lasing leads to a more rapid increase in FWHM. We observed a continuous blueshift of the emission peak of up to $\approx$5 meV, which is another characteristic feature of polariton lasing. This value is at an intermediate range in between what has been observed in the ladder-type conjugated polymer (MeLPPP) cavity[6] and our previous work on fluorene-based cavities.[18,20] This blueshift may result from multiple reasons, including repulsive self-interaction among
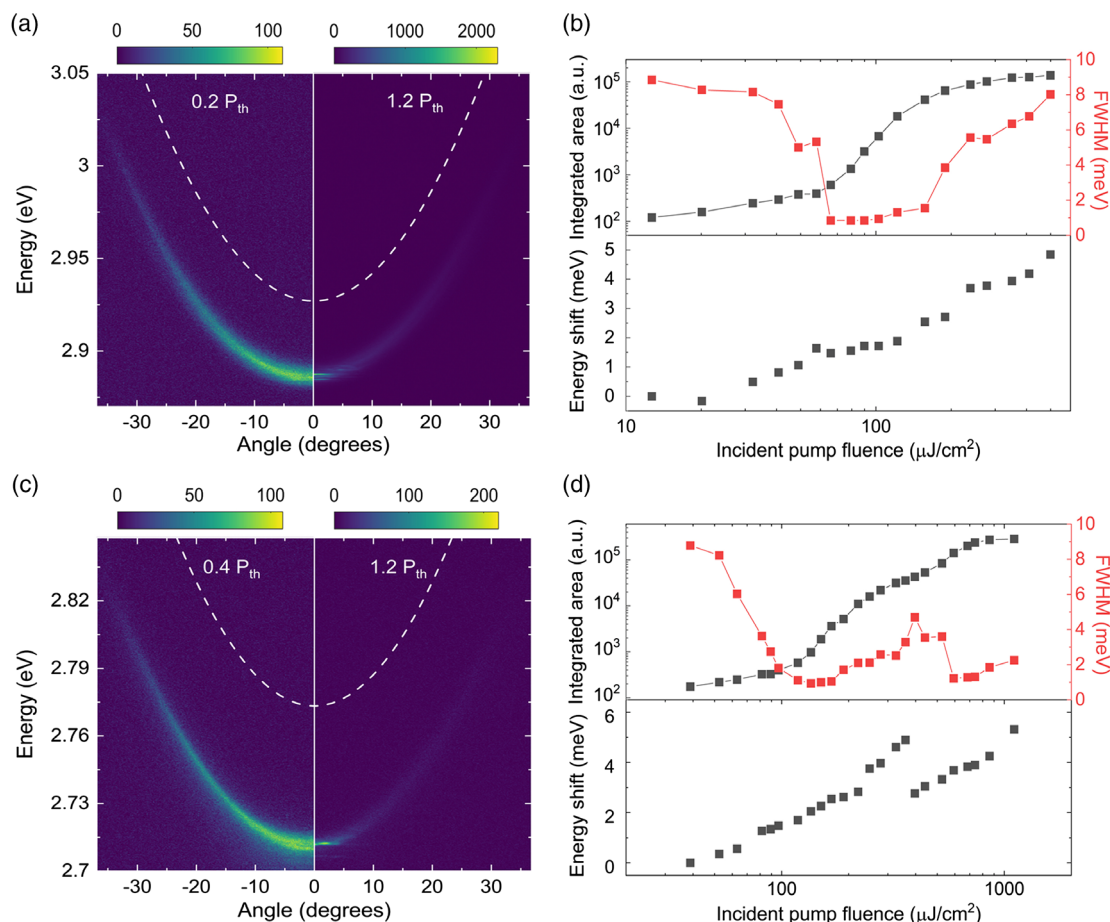
**ADVANCED
SCIENCE NEWS**
www.advancedsciencenews.com

**ADVANCED
PHOTONICS
RESEARCH**
Open Access
www.adpr-journal.com

Figure 3. Angle-resolved PL of a) 2L-F and c) 4L-F microcavities below (left half) and above (right half) threshold. Note that color scales are different for each panel as indicated. White dashed lines indicate the uncoupled cavity photon modes. The integrated area and the FWHM of emission spectrum of b) 2L-F and d) 4L-F microcavities at $k_{//} = 0$ and the blueshift of emission peak as a function of pump fluence.

polaritons,[6,19,21,23,35] gradual saturation of molecular optical transitions, and intermolecular energy migration.[36]

Similar plots for the 4L-F cavity are shown in Figure 3d. From the evolution of the integrated emission spectra at $k_{//} = 0$ in Figure S4d–f, Supporting Information, the incident threshold of the 4L-F cavity is found to be 109 μJ cm^{-2}. The nonlinear increase of integrated intensity is accompanied by a linewidth narrowing of emission spectra from 8.8 to 0.9 meV and a blueshift of around 5 meV, which is of the same size as that observed in the 2L-F cavity. It is evident in Figure 3d that the 4L-F data show a fluctuation in the integrated area and the FWHM and a concurrent discontinuity in the energy shift for a pump density of 396 μJ cm^{-2}. Note that Figure 3d plots the overall FWHM of the multi-mode PL spectra. The first broadening of FWHM with increasing pump fluence is attributed to a polariton decoherence process (where a single mode broadens in spectrum), before there is an appearance and merger of multiple distinct lasing modes. Following a mode hop of the most intense peak, a new dominant mode emerges that rebroadens when pump the cavity is far above threshold. Figure S5, Supporting Information, more clearly shows that the dominant peak of the 4L-F cavity is at 456.8 nm when excited at 360 μJ cm^{-2}

and hops to 457.2 nm when the pump fluence increased to 396 μJ cm^{-2}. This is attributed to competition between multiple spatial modes due to disorder in cavity thickness within the excitation area.[5] The absorbed pump fluence thresholds of polariton lasing were estimated from the incident thresholds by taking consideration of the round-trip transmittance of the bottom and top DBRs and the absorbance of the active layers. Absorbed pump fluence thresholds for 2L-F and 4L-F are 12 and 17 μJ cm^{-2}, respectively, comparable with the lowest absorbed threshold that was reported for a fluorene oligomer.[20] It is also useful to compare the results with MeLPPP that has been reported to show polariton lasing.[6] Incident fluence thresholds of the 2L-F and 4L-F cavities are only one-eighth and one-fifth of that reported for an MeLPPP cavity with similar photon lifetime. Although the PLQYs of the ladder-type oligo(*p*-phenylene)s are similar to the polymer, the peak absorption coefficients of 2L-F and 4L-F are 1.5 times higher than that of $S_{0,\nu=0} \rightarrow S_{1,\nu=0}$ transition in MeLPPP,[37] which may be due to a denser packing of the oligomers in the film.

It is noticeable that the incident threshold of the 4L-F cavity is higher than that of the 2L-F cavity, whereas the absorbed thresholds are very similar. The primary reason is because the

**ADVANCED
SCIENCE NEWS**

www.advancedsciencenews.com

**ADVANCED
PHOTONICS
RESEARCH**

www.adpr-journal.com

absorption coefficient at the excitation wavelength of the 2L-F film (3.0×10^4 cm^{-1}) is more than twice of that of the 4L-F film (1.3×10^4 cm^{-1}). Thus, the exciton bath can more effectively populate the LPB in the 2L-F cavity. In addition, as the rigidity of 4L-F increases via π-conjugation, the integration of more phenylene units diminishes the molecular solubility. It reflects on the inhomogeneity of the cavity thickness and, therefore, more disordered emission spectra of polariton condensates, as shown in Figure S5, Supporting Information. Other possible reasons responsible for the high threshold in the 4L-F cavity include the exciton quenching due to the large coplanar π-conjugated system.[27] Also, increased structural planarity can give rise to solid-state packing, which may lead to exciton–exciton annihilation. Therefore, although 4L-F with more rigid molecular structure shows a larger Rabi splitting compared with 2L-F, structural defects of the film lead to a higher polariton lasing threshold in the cavity.[38]

Figure 4 shows the spatial interferograms of a 2L-F cavity and a 4L-F cavity pumped above threshold (1.2 P_{th}) at 79 and 135 μJ cm^{-2}, respectively, using a Michelson interferometer equipped with a retroreflector to invert the real space image to interfere with the original from the microcavity. This configuration has been used in previous studies to explore either spatial or temporal coherence in polariton condensates.[30–32,39–41] Clear fringes are observed in both 2L-F and 4L-F cavities over a distance up to 5 μm, indicating that long-range spatial coherence builds up when the polaritons macroscopically accumulate at the bottom of LPBs. Real space images from the individual arms of the interferometer are shown in Figure S6 and S7, Supporting Information. The beam collapses to a small spot of size ≈5 μm, which limits the spatial extent of the fringes. There are no fringes in the overlapped real space images below threshold, excluding the possibility that the fringes originated from the excitation laser pulses.

3. Conclusions

In conclusion, we observe room temperature polariton lasing from two ladder-type oligo(p-phenylene) molecules, 2L-F and

4L-F, with different π-conjugation lengths. The absorbed thresholds for 2L-F and 4L-F cavities are 12 and 17 μJ cm^{-2}, respectively, which are comparable to the lowest absorbed threshold that has been reported for organic semiconductors in a planar cavity structure.[20] With longer π-conjugation length, the more rigid 4L-F molecule shows spectrally resolved vibronic replicas, which leads to an increased Rabi splitting of the UPB and LPB. Polariton lasing in these two cavities is evidenced by a nonlinear increase of the spectrally integrated emission, around tenfold reduction of spectral linewidth, blueshift of emission peaks, and buildup of long-range spatial coherence above excitation thresholds. By extending the backbone of oligo(p-phenylene)s, the polariton lasing wavelength shifts from ≈430 nm in 2L-F cavity to ≈457 nm in 4L-F cavity, manifesting that this novel family of molecules are promising materials for achieving polariton lasing at low thresholds and tunable wavelength by tailoring conjugation length.

4. Experimental Section

Sample Fabrication: 2L-F and 4L-F were synthesized as described elsewhere.[27] The molecules were dissolved in toluene at the concentrations of 20 mg mL^{-1} for 2L-F and 18 mg mL^{-1} for 4L-F and stirred at 60 °C on a hot plate overnight. Bare film measurements, including absorption, PL, PLQY, and ellipsometry, were performed on spin-coated films on fused silica substrates.

The microcavities were configured with 11.5 pairs of Ta$_2$O$_5$/SiO$_2$ as bottom DBRs deposited by radiofrequency magnetron sputtering on precleaned fused silica substrates. The thicknesses of the alternating Ta$_2$O$_5$ and SiO$_2$ layers were set to be $\lambda/4n$, where λ is the center wavelength of the DBR stop band (varying according to the active organic layer), and n is the refractive index of Ta$_2$O$_5$ or SiO$_2$ at the center wavelength. The core of the microcavity is composed of the spin-coated organic film, sandwiched between thermally evaporated layers (20 nm thick) of LiF, deposited on bottom DBRs. All microcavities were completed by sputtering 8.5 pairs of Ta$_2$O$_5$ and SiO$_2$ with the same layer thicknesses as the bottom DBRs on top of the LiF layer. The whole process, including the fabrication of bare films and microcavities, was conducted in a nitrogen filled glovebox to exclude oxygen from the organic layer.

Characterization: The absorption spectra of 2L-F and 4L-F bare films were measured with a Cary-300 UV–Vis spectrophotometer, and the PL spectra were collected using an Edinburgh Instruments FLS980
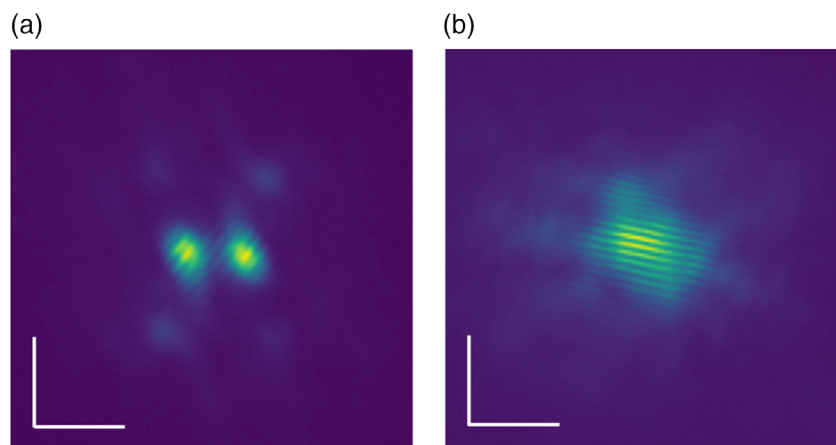

(a)　　　(b)

Figure 4. Interferograms recorded by a Michelson interferometer for a) 2L-F cavity and b) 4L-F cavity at 1.2 P_{th} (=79 and 135 μJ cm^{-2}, respectively). All scale bars are 5 μm.

spectrometer. The PLQY measurements of the two compounds in the solid state were performed in an integrating sphere in a Hamamatsu Photonics C9920-02 system.[42] The optical constants and thickness of bare films were measured by spectroscopic ellipsometry (J.A. Woollam Co., Inc. M-2000DI). Polarized angle-resolved reflectivity measurements of microcavities were also performed on a J.A. Woollam ellipsometer using a dual deuterium and quartz tungsten halogen white light source. A motorized sample platform and detection arm were used to record reflectivity spectra from $20°$ to $74°$.

Angle-resolved PL measurements were conducted using a Fourier imaging microscope in transmission geometry. Microcavities were excited non-resonantly close to normal incidence by a laser beam at 343 nm from the substrate side. The vertically polarized pulsed pump laser was generated as the third harmonic of a Light Conversion Pharos laser with a pulse duration of 200 fs and a repetition rate of 5 kHz. The Gaussian laser beam size was measured to be 46 ± 3 µm in diameter using a beam profiler (Lasercam HR, Coherent). The emitted light from microcavities was collected by a Nikon S Plan Fluor extra-long working distance (ELWD) 40× microscope objective with a numerical aperture of 0.6 and detected by an Andor Shamrock SR500i charge-coupled device (CCD) spectrometer. PL was resolved in both spectra and angle using an 1800 grooves mm^{-1} grating resulting in a spectral resolution of ≈ 0.0125 nm. A 400 nm long-pass filter was placed at the entrance of the CCD spectrometer to cut off any residual signal from the pump laser. An external diaphragm shutter was synchronized with the CCD spectrometer to transmit the laser beam only during the data acquisition process.

Spatial coherence measurements were performed using a home-built Michelson interferometer with one arm replaced by a hollow retroreflector. PL from microcavities was collimated by the Nikon S Plan Fluor ELWD 40× microscope objective and then split into two paths into the interferometer by passing through a 50:50 non-polarizing beam splitter cube. The inverted emission spot from the retroreflector arm and the reflected emission spot from the other arm then passed through a plano-convex lens and were combined on the CCD spectrometer. A 400 nm long-pass spectral filter was used to remove background light from the excitation laser. The coherence and angle-resolved PL measurements were carried out at room temperature in air.

Supporting Information

Supporting Information is available from the Wiley Online Library or from the author.

Acknowledgements

Conflict of Interest

The authors declare no conflict of interest.

Keywords

[1] A. Kavokin, J. J. Baumberg, G. Malpuech, F. P. Laussy, *Microcavities*, Oxford University Press, Oxford, UK **2017**.

[2] A. Imamoğlu, R. J. Ram, S. Pau, Y. Yamamoto, *Phys. Rev. A* **1996**, *53*, 4250.

[3] G. Weihs, H. Deng, D. Snoke, Y. Yamamoto, *Phys. Status Solidi Appl. Res.* **2004**, *201*, 625.

[4] A. Das, J. Heo, M. Jankowski, W. Guo, L. Zhang, H. Deng, P. Bhattacharya, *Phys. Rev. Lett.* **2011**, *107*, 066405.

[5] P. Bhattacharya, T. Frost, S. Deshpande, M. Z. Baten, A. Hazari, A. Das, *Phys. Rev. Lett.* **2014**, *112*, 29.

[6] J. D. Plumhof, T. Stoeferle, L. Mai, U. Scherf, R. Mahrt, *Nat. Mater.* **2014**, *13*, 328.

[7] A. Amo, J. Lefrère, S. Pigeon, C. Adrados, C. Ciuti, I. Carusotto, R. Houdré, E. Giacobino, A. Bramati, *Nat. Phys.* **2009**, *5*, 805.

[8] S. Christopoulos, G. B. H. Von Högersthal, A. J. D. Grundy, P. G. Lagoudakis, A. V. Kavokin, J. J. Baumberg, G. Christmann, R. Butté, E. Feltin, J. F. Carlin, N. Grandjean, *Phys. Rev. Lett.* **2007**, *98*, 126405.

[9] T.-C. Lu, Y.-Y. Lai, Y.-P. Lan, S.-W. Huang, J.-R. Chen, Y.-C. Wu, W.-F. Hsieh, H. Deng, *Opt. Express* **2012**, *20*, 5530.

[10] R. Su, S. Ghosh, J. Wang, S. Liu, C. Diederichs, T. C. H. Liew, Q. Xiong, *Nat. Phys.* **2020**, *16*, 301.

[11] R. Su, C. Diederichs, J. Wang, T. C. H. Liew, J. Zhao, S. Liu, W. Xu, Z. Chen, Q. Xiong, *Nano Lett.* **2017**, *17*, 3982.

[12] G. Lanty, A. Bréhier, R. Parashkov, J. S. Lauret, E. Deleporte, *New J. Phys.* **2008**, *10*, 065007.

[13] N. H. M. Dang, D. Gerace, E. Drouard, G. Trippé-Allard, F. Lédeé, R. Mazurczyk, E. Deleporte, C. Seassal, H. S. Nguyen, *Nano Lett.* **2020**, *20*, 2113.

[14] J. Wang, R. Su, J. Xing, D. Bao, C. Diederichs, S. Liu, T. C. H. Liew, Z. Chen, Q. Xiong, *ACS Nano* **2018**, *12*, 8382.

[15] A. Fieramosca, L. Polimeno, V. Ardizzone, L. De Marco, M. Pugliese, V. Maiorano, M. De Giorgi, L. Dominici, G. Gigli, D. Gerace, D. Ballarini, D. Sanvitto, *Sci. Adv.* **2019**, *5*, 1.

[16] D. G. Lidzey, D. D. C. Bradley, M. S. Skolnick, T. Virgili, S. Walker, D. M. Whittaker, *Nature* **1998**, *395*, 53.

[17] S. Kéna-Cohen, S. R. Forrest, *Nat. Photonics* **2010**, *4*, 371.

[18] M. Wei, S. K. Rajendran, H. Ohadi, L. Tropf, M. C. Gather, G. A. Turnbull, I. D. W. Samuel, *Optica* **2019**, *6*, 1124.

[19] K. S. Daskalakis, S. A. Maier, R. Murray, S. Kéna-Cohen, *Nat. Mater.* **2014**, *13*, 271.

[20] S. K. Rajendran, M. Wei, H. Ohadi, A. Ruseckas, G. A. Turnbull, I. D. W. Samuel, *Adv. Opt. Mater.* **2019**, *7*, 1801791.

[21] C. P. Dietrich, A. Steude, L. Tropf, M. Schubert, N. M. Kronenberg, K. Ostermann, S. Höfling, M. C. Gather, *Sci. Adv.* **2016**, *2*, e1600666.

[22] S. Betzold, M. Dusel, O. Kyriienko, C. P. Dietrich, S. Klembt, J. Ohmer, U. Fischer, I. A. Shelykh, C. Schneider, S. Höfling, *ACS Photonics* **2020**, *7*, 384.

[23] T. Cookson, K. Georgiou, A. Zasedatelev, R. T. Grant, T. Virgili, M. Cavazzini, F. Galeotti, C. Clark, N. G. Berloff, D. G. Lidzey, P. G. Lagoudakis, *Adv. Opt. Mater.* **2017**, *5*, 1700203.

[24] D. Sannikov, T. Yagafarov, K. Georgiou, A. Zasedatelev, A. Baranikov, L. Gai, Z. Shen, D. Lidzey, P. Lagoudakis, *Adv. Opt. Mater.* **2019**, *7*, 1900163.

[25] U. Scherf, *J. Mater. Chem.* **1999**, *9*, 1853.

[26] S. F. Alvarado, S. Barth, H. Bässler, U. Scherf, J. W. Van Der Horst, P. A. Bobbert, M. A. J. Michels, *Adv. Funct. Mater.* **2002**, *12*, 117.

[27] M. Fang, J. Huang, S. J. Chang, Y. Jiang, W. Y. Lai, W. Huang, *J. Mater. Chem. C* **2017**, *5*, 5797.

[28] L. S. Hung, L. S. Liao, C. S. Lee, S. T. Lee, *J. Appl. Phys.* **1999**, *86*, 4607.

[29] A. Holländer, M. Haupt, C. Oehr, *Plasma Process. Polym.* **2007**, *4*, 773.

[30] R. Houdré, R. P. Stanley, M. Ilegems, *Phys. Rev. A* **1996**, *53*, 2711.

[31] J. A. Cwik, P. Kirton, S. De Liberato, J. Keeling, *Phys. Rev. A* **2016**, *93*, 033840.

[32] J. Kasprzak, M. Richard, S. Kundermann, A. Baas, P. Jeambrun, J. M. J. Keeling, F. M. Marchetti, M. H. Szymánska, R. André, J. L. Staehli, V. Savona, P. B. Littlewood, B. Deveaud, L. S. Dang, *Nature* **2006**, *443*, 409.

[33] D. Porras, C. Tejedor, *Phys. Rev. B* **2003**, *67*, 161310.

[34] S. Kim, B. Zhang, Z. Wang, J. Fischer, S. Brodbeck, M. Kamp, C. Schneider, S. Höfling, H. Deng, *Phys. Rev. X* **2016**, *6*, 011026.

[35] M. Vladimirova, S. Cronenberger, D. Scalbert, K. V. Kavokin, A. Miard, A. Lemaître, J. Bloch, D. Solnyshkov, G. Malpuech, A. V. Kavokin, *Phys. Rev. B* **2010**, *82*, 075301.

[36] T. Yagafarov, D. Sannikov, A. Zasedatelev, K. Georgiou, A. Baranikov, O. Kyriienko, I. Shelykh, L. Gai, Z. Shen, D. Lidzey, P. Lagoudakis, *Commun. Phys.* **2020**, *3*, 18.

[37] A. Rudnick, K. J. Kass, E. Preis, U. Scherf, H. Bässler, A. Köhler, *J. Chem. Phys.* **2017**, *146*, 174903.

[38] J. Keeling, S. Kéna-Cohen, *Annu. Rev. Phys. Chem.* **2020**, *71*, 435.

[39] G. Roumpos, M. Lohse, W. H. Nitsche, J. Keeling, M. H. Szymańska, P. B. Littlewood, A. Löffler, S. Höfling, L. Worschechh, A. Forchel, Y. Yamamoto, *Proc. Natl. Acad. Sci. U. S. A.* **2012**, *109*, 6467.

[40] K. S. Daskalakis, S. A. Maier, S. Kénna-Cohen, *Phys. Rev. Lett.* **2015**, *115*, 035301.

[41] D. Caputo, D. Ballarini, G. Dagvadorj, C. S. Muñoz, M. De Giorgi, L. Dominici, K. West, L. N. Pfeiffer, G. Gigli, F. P. Laussy, M. H. Szymanska, D. Sanvitto, *Nat. Mater.* **2018**, *17*, 145.

[42] N. C. Greenham, I. D. W. Samuel, G. R. Hayes, R. T. Phillips, Y. A. R. R. Kessener, S. C. Moratti, A. B. Holmes, R. H. Friend, *Chem. Phys. Lett.* **1995**, *241*, 89.

[43] M. Wei, S. K. Rajendran, M. Fang, W. Lai, G. A. Turnbull, I. D. W. Samuel, *Dataset. University of St Andrews Research Portal* **1995**, http://doi.org/10.17630/7bd2b281-2ae9-4de8-a091-4f409cbe7cb1.